Article

Study of the Resistance of Lithium-Containing Ceramics to Helium Swelling

Artem L. Kozlovskiy [1,2,*], Dmitriy I. Shlimas [1,2], Daryn B. Borgekov [1,2] and Maxim V. Zdorovets [1,2]

1   Laboratory of Solid State Physics, The Institute of Nuclear Physics, Almaty 050032, Kazakhstan; shlimas@mail.ru (D.I.S.); mzdorovets@gmail.com (M.V.Z.)
2   Engineering Profile Laboratory, L.N. Gumilyov Eurasian National University, Astana 010008, Kazakhstan
*   Correspondence: kozlovskiy.a@inp.kz; Tel.: +7-702-441-3368; Fax:+7-702-441-3368

Abstract: The paper presents the results of studies of the resistance of lithium ceramics to helium swelling during its accumulation in the structure of the near-surface layer, and the identification of the three types of lithium ceramics most resistant to radiation degradation: Li_4SiO_4, Li_2TiO_3, and Li_2ZrO_3. The simulation of helium swelling under high-dose irradiation was carried out by irradiation with He^{2+} ions with fluences of 1×10^{16} ion/cm^2–5×10^{17} ion/cm^2, which allows for simulating the implanted helium accumulation with a high concentration in the damaged surface layer (about 500 nm thick). The samples were irradiated at a temperature of 1000 K, the choice of which was determined by the possibility of simulating radiation damage as close as possible to real operating conditions. Such accumulation can result in the formation of gas-filled bubbles. Through the application of X-ray phase analysis, indentation testing, and thermophysical parameter assessments, it was ascertained that among the three ceramic types, Li_4SiO_4 ceramics exhibit the highest resistance to helium-induced swelling. These ceramics experienced less significant alterations in their properties compared to the other two types. An analysis of the correlation between the structural and strength parameters of lithium-containing ceramics revealed that the most significant changes occur when the volumetric swelling of the crystal lattice becomes the dominant factor in structural alterations. This phenomenon is manifested as an accelerated degradation of strength characteristics, exceeding 10%. At the same time, analysis of these alterations in the stability of thermophysical parameters to the accumulation of structural distortions revealed that, regardless of the type of ceramics, the degradation of thermophysical properties is most pronounced under high-dose irradiation (above 10^{17} ion/cm^2).

Keywords: lithium ceramics; radiation embrittlement; gas swelling; degradation; tritium; strength properties

1. Introduction

One of the directions for advancing the energy sector in both developed and developing nations, with the aim of reducing reliance on hydrocarbons and fossil fuels while elevating hydrocarbon neutrality, involves the exploration of new alternative energy sources, including nuclear and thermonuclear energy. In recent years, significant emphasis has been placed on research related to the development of novel blanket materials centered on lithium-containing ceramics [1–3]. These materials hold the potential to address the challenge of producing and accumulating tritium, the primary fuel for the thermonuclear cycle [4,5]. Numerous technological options are presently under examination for tritium production. Among these options is the utilization of lithium-containing ceramics, which generate tritium when subjected to neutron irradiation during nuclear reactions [6,7]. Furthermore, due to its mobility, tritium can be extracted from ceramics and promptly employed to sustain a thermonuclear reaction. However, during neutron-induced nuclear reactions with lithium, helium is concurrently generated [8,9]. The accumulation

of helium within the ceramic structure can also result in its destabilization. At the same time, destabilization processes are associated primarily with the accumulation of helium in the near-surface layer of ceramics [10,11]. This is attributed to helium's notable mobility, as it rapidly migrates along grain boundaries in ceramics and alloys. Furthermore, helium can agglomerate by filling voids or cavities within the structure. These helium accumulation processes are accompanied by an escalation of deformation distortions in the structure, a consequence of ionization processes and helium movement within the structure [12–14]. As a consequence of these mechanisms, ceramics undergo detrimental changes in their properties. These changes include a decline in their strength characteristics, such as reduced hardness, heightened susceptibility to cracking, and increased susceptibility to fractures even under minor external pressures. Additionally, there is a degradation in thermophysical properties attributable to an elevation in scattering factors during the phonon-based heat transfer mechanism. It is noteworthy to mention that in the context of nuclear reactions between lithium and tritium, helium accumulation as shown in several works [15,16], exhibits a non-linear behavior over time, often occurring abruptly and leading to gas emissions, including helium, hydrogen, and tritium. This observation suggests that the mechanisms behind helium accumulation and subsequent swelling are not fully comprehended, necessitating further detailed experimentation.

One of the ways to study gas swelling in the near-surface layer is the method of simulation of these processes by ion irradiation, which allows, in a fairly short time, for the accumulation of sufficiently large concentrations of implanted helium in the near-surface layer, which can result in swelling and destruction [17–19]. To conduct such experiments, heavy ion accelerators are used, which makes it possible to simulate the gas swelling processes and evaluate the kinetics of swelling and degradation processes by varying irradiation conditions, in particular, irradiation fluence and particle flux density [20,21]. Furthermore, the use of irradiation modes at elevated temperatures, characteristic of operating temperature conditions, makes it possible to simulate the kinetic processes of destruction of ceramics during the accumulation of helium in the surface layer and its subsequent destruction, the analysis of which will subsequently make it possible to predict the behavior of ceramic materials under real operating conditions [22–25].

The purpose of this research is to study the radiation damage processes and the consequences caused by them in lithium-containing ceramics Li_4SiO_4, Li_2TiO_3, and Li_2ZrO_3, to assess the irradiation effect on changes in the mechanical strength and thermophysical parameters's stability. The findings from this study will facilitate a comprehensive assessment of the resistance of different lithium-containing ceramics against radiation-induced damage. Ultimately, this assessment will help identify the most robust ceramics for potential use as the foundation for blanket materials intended for tritium propagation.

2. Materials and Methods

2.1. Characterization of Initial Ceramic Samples

The selection of Li_4SiO_4, Li_2TiO_3, and Li_2ZrO_3, characterized by their monoclinic crystal structure, as the subjects of investigation stems from their potential suitability as tritium breeding materials—a crucial component in the context of thermonuclear energy as a potential fuel source. These ceramic types were synthesized through a mechanochemical mixing process of the initial components, followed by subsequent thermal sintering of the resultant mixtures. This sintering was conducted in a muffle furnace at a temperature of 1000 °C for a duration of 5 h, aiming to produce structurally ordered ceramics characterized by a monoclinic crystalline structure. Figure 1 illustrates the X-ray diffraction patterns of the synthesized ceramics, namely, Li_4SiO_4, Li_2TiO_3, and Li_2ZrO_3, in their pristine, pre-irradiated condition.
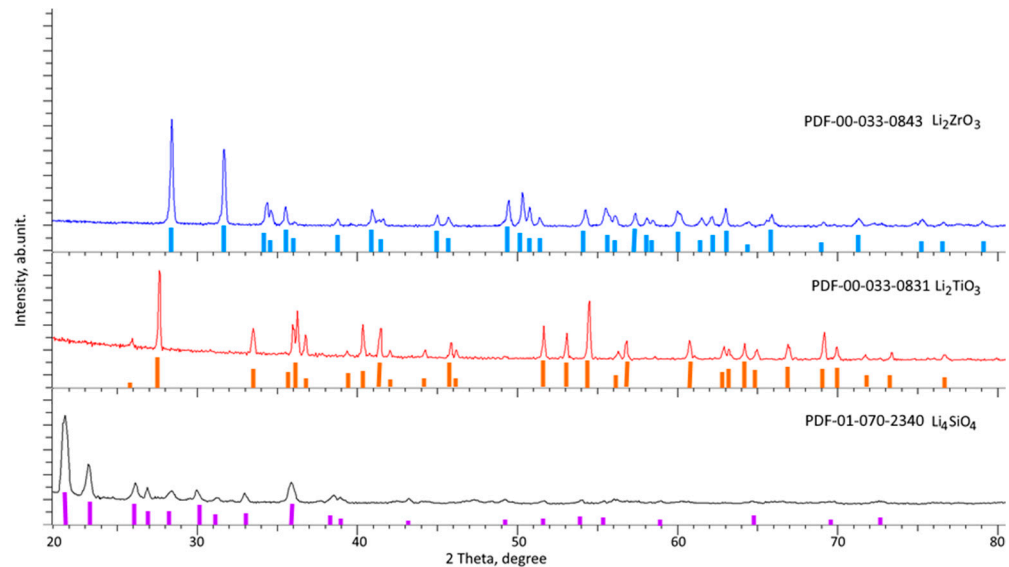
Figure 1. X-ray diffraction patterns of the studied Li_4SiO_4, Li_2TiO_3, and Li_2ZrO_3 ceramics in the initial state, obtained using the mechanochemical synthesis method.

Based on the X-ray phase analysis findings, it was determined that the ceramics in question, produced from a blend of SiO_2 and $LiClO_4 \cdot 3H_2O$ compounds followed by subsequent thermal annealing, exhibit a monoclinic structure with crystal lattice parameters of a = 11.54015 ± 0.00042 Å, b = 6.07448 ± 0.00053 Å, c = 16.60257 ± 0.00024 Å, β = 99.285°, V = 1147.60 Å^3, characterized by a high degree of structural order exceeding 90%. For ceramics derived through the process of mechanochemical grinding followed by thermal annealing of a blend comprising TiO_2 and $LiClO_4 \cdot 3H_2O$ compounds, the phase composition of the ceramics is a monoclinic phase with parameters of a = 5.05409 ± 0.00018 Å, b = 8.76622 ± 0.00014 Å, c = 9.73412 ± 0.00032 Å, β = 100.141°, V = 424.54 Å^3, and a degree of structural ordering of 93%. For ceramics obtained from ZrO_2 and $LiClO_4 \cdot 3H_2O$ compounds, the observed position of diffraction reflections, as well as the ratio of their intensity, is characteristic of a monoclinic phase with parameters a = 5.39574 ± 0.00017 Å, b = 8.98502 ± 0.00018 Å, c = 5.38123 ± 0.00031 Å, β = 113.132°, V = 239.91 Å^3, and a degree of structural ordering of 92.5%. To determine the phase composition, a PDF-2(2016) database was used, from which the most suitable card values were selected for the observed phases Li_4SiO_4 (PDF-01-070-2340) monoclinic type of structure, spatial system P21/m(11), Li_2TiO_3 (PDF-00-033-0831) monoclinic type of structure, spatial system C2/c(15), Li_2ZrO_3 (PDF-00-033-0843) monoclinic type of structure, spatial system C2/c(15). The structural ordering degree was determined by calculating the ratio of the weight contributions of diffraction reflections and background radiation characteristic of disordered inclusions in ceramics. Refinement of the crystal lattice parameters was carried out by calculating the position of the maxima and the subsequent determination of their characteristic interplanar distances, knowing which, using the Nelson–Taylor technique, it is possible to determine the parameters and volume of the crystal lattice.

2.2. Simulation of Helium Swelling

The specimens underwent irradiation at the DC-60 accelerator to simulate helium swelling processes within the surface layer, contingent upon the concentration of implanted helium during high-dose irradiation. To simulate these processes, low-energy He^{2+} ions with an energy level of 40 keV were used. The irradiation process was conducted at a temperature of 1000 K, striving to closely mimic the operating conditions of these ceramic types during tritium production. In this scenario, the selection of the irradiation temperature aligns with preliminary information regarding blanket operational conditions. Furthermore, in contrast to irradiation at room temperature, subjecting samples to irradiation at elevated

temperatures can accelerate the helium migration processes within the damaged layer due to the enhanced mobility of the crystal structure. However, under these circumstances, the accelerated migration of implanted helium can result in its release through the pores within the ceramic structure, potentially leading to an augmentation of deformation distortions within the damaged layer. Irradiation fluences (1×10^{16} ion/cm^2–5×10^{17} ion/cm^2) were selected considering the possibility of achieving the effect of deep overlap of defective areas (5–10 dpa) and implanted helium concentrations of the order of several at. %.

Figure 2 displays the results of assessing the ionization losses of He^{2+} ions during the interaction with the crystal structure of lithium-containing ceramics, obtained by simulation using the SRIM Pro 2013 software code. The Kinchin–Pease model, which takes into account cascade collisions during the interaction of incident ions with the crystal structure of the target and the formation of vacancy defects, was applied. The number of collisions was chosen to be more than 10,000, which made it possible to determine with good accuracy and statistical data the magnitude of ionization losses of incident ions during the interaction with the crystal structure.
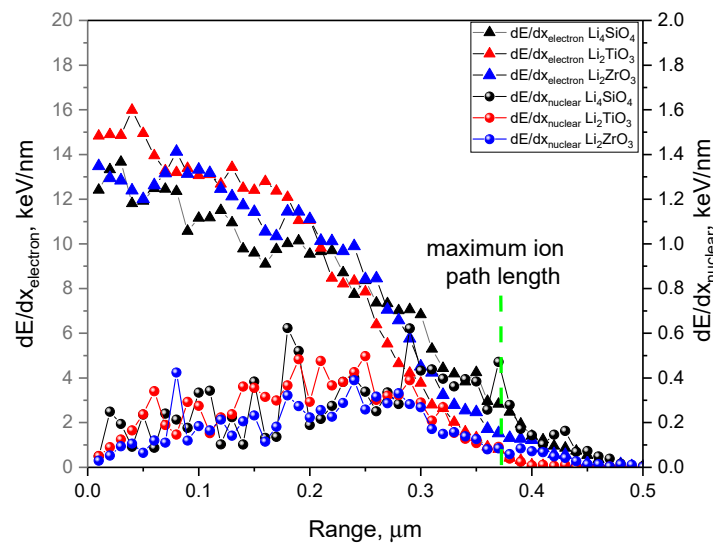
Figure 2. The assessment results of ionization losses of He^{2+} ions during the interaction with the crystal structure of lithium-containing ceramics.

As is evident from the data presented, the maximum value of ionization losses of incident He^{2+} ions during the interaction with the electronic subsystem is 12–14 keV/nm, while the value of nuclear losses of He^{2+} during the interaction with nuclei is no more than 0.3–0.4 keV/nm. Thus, by estimating the weight contributions of ionization losses in a near-surface layer with a thickness of 0.35–0.4 µm, it becomes apparent that the most significant alterations in ceramic properties are attributable to ionization processes in the electronic subsystem, fluctuations in electron density within the damaged layer, and the cascade effects of secondary electrons.

Figure 3 presents estimated calculations of the distribution of atomic displacement values in a damaged layer of a 0.5 µm thick ceramic depending on the irradiation fluence, which characterizes the accumulation of structural damage caused by the interaction of incident ions with matter. The calculations considered the formation of vacancies in the damaged layer structure, alongside cascade effects. Based on the data provided, it is evident that the maximum value of atomic displacements for all three ceramics in the study reaches approximately 7.0–8 dpa at the highest irradiation fluence of 5×10^{17} ion/cm^2, signifying a substantial accumulation of structural distortions within the damaged layer. It is noteworthy that the distribution of structural damage, as indicated by the value of atomic displacements along the ion trajectory, follows a bell-shaped pattern, with the peak occurring within the 0.3–0.35 µm range. This corresponds to the region characterized by

the predominance of ionization losses incurred by incident ions during their interaction with nuclei. The presented data comparing the profiles of atomic displacement values along the trajectory of ion motion at the maximum irradiation fluence (5×10^{17} ion/cm^2) in Figure 3d clearly reflect the difference in the profiles of radiation damage in ceramics, as well as the maximum displacement value achieved at the maximum. According to the calculated data, the maximum displacement value above 8 dpa at maximum fluence is achieved for Li$_4$SiO$_4$ ceramics, while the displacement value for Li$_2$TiO$_3$ and Li$_2$ZrO$_3$ ceramics is 6.8–7.5 dpa. At the same time, the difference in the displacement values under the same irradiation conditions (initial ion energy) can be explained by differences in the density of the ceramics, as well as the values of the binding energy of atoms in the ceramics. In turn, analyzing the data on the profiles of atomic displacement values, we can conclude that the accumulation of this quantity has a clearly asymmetric shape along the trajectory, reaching a maximum in the region of 0.3–0.35 μm (with a slight shift of up to 0.35–0.4 μm for Li$_4$SiO$_4$ ceramics), which corresponds to the maximum nuclear ionization losses of incident He^{2+} ions in ceramics. The decrease in the value of the amohmic displacements after the maximum can be explained by effects associated with the inhibition of ions in the target material, as well as by diffusion processes. The very shape of the distribution, which has an asymmetric bell shape, is explained by the dependencies of changes in the processes of the interaction of incident ions with the target material. At the initial stages of interaction (at a travel depth of 0.1–0.2 μm), the main contribution to structural changes is made by electronic ionization losses arising from the interaction of incident ions with electron shells. In the case when the value of electronic ionization losses declines due to braking effects, nuclear ionization losses that arise during the interaction of incident ions with nuclei, forming primarily knocked out atoms and vacancies, begin to have a greater influence in the processes of the interaction of ions with the crystal structure.

(a)　　　　　　　　　(b)　　　　　　　　　(c)

(d)
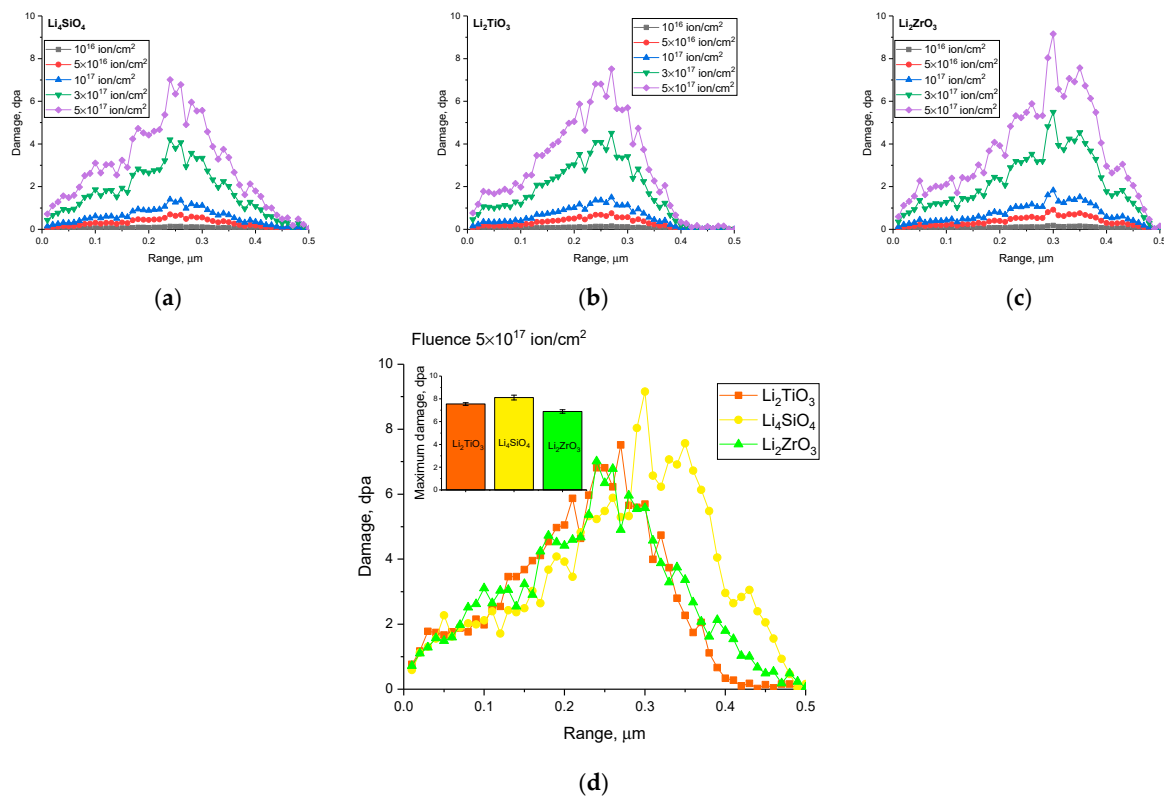
Figure 3. The assessment results of the value of atomic displacements along the trajectory of ion movement in the near-surface layer of ceramics as a function of the irradiation fluence: (**a**) Li$_4$SiO$_4$; (**b**) Li$_2$TiO$_3$; (**c**) Li$_2$ZrO$_3$; (**d**) graph comparing the values of atomic displacements along the trajectory of movement of He^{2+} ions in ceramics at an irradiation fluence of 5×10^{17} ion/cm^2.

The study of the effect of irradiation and the subsequent accumulation of implanted helium on alterations in the strength characteristics of ceramics was conducted by assessing the hardness and crack resistance of ceramics. The data were presented in the form of dependencies of variations in strength parameters on irradiation fluence for all studied combinations of ceramic compositions. Hardness determination was carried out via a LECO LM700 microhardness tester (LECO, Tokyo, Japan). Indentation was performed using a Vickers diamond pyramid, with a constant load on the indenter equal to 100 N. The indentation time was 15 s, after which the hardness value was determined using visual methods for determining the diagonals of the indentation, followed by the application of conversion formulas. The choice of indentation conditions was due to the ability to measure the hardness of the entire damaged layer (depth 0.3–0.4 µm), since at these loads the maximum penetration depth of the indenter does not exceed this value. Hardness measurements were carried out by successive measurements of indentation of the surface of a ceramic sample in different areas (more than 20 measurements per sample), which made it possible to determine the average hardness value, as well as the standard deviation. At the same time, the measurements were carried out in such a way that each previous indenter print did not affect the subsequent measurement (a distance of about 50–70 µm was maintained between the indenter prints). The number of indentation measurements made it possible to establish the uniformity of changes in the strength properties of ceramics, as well as to determine changes in the diagonals of the indenter. Based on changes in the indenter imprint diagonals c/a (c is the crack half length, and a is the indenter imprint semi-diagonal), as well as the hardness value using formula (1), it is possible to estimate the value of the critical stress intensity factor (K_{1c}) in the samples, which reflects the change in fracture toughness (crack resistance):

$$K_{1c} = 0/16 \times H \times a^{1/2} \times (c/a)^{-3/2} \tag{1}$$

where H is the Vickers hardness value, c is the half length of the crack, and a is the half diagonal of the indenter imprint.

To determine the resistance to cracking due to the accumulated structural distortion, the single compression method was chosen and implemented using a testing machine (Walter + Bai AG, Löhningen, Switzerland). Single compression tests were conducted following a conventional procedure to detect the onset of microcrack formation in specimens subjected to a constant loading rate. Monitoring of crack formation was achieved through an extensometer, along with tracking alterations in the applied load on the specimen.

The study of thermophysical parameters, alongside the resulting heat losses during the accumulation of radiation damage in lithium-containing ceramics that occurs during swelling and destruction as a result of helium agglomeration, was carried out using the method of determining the longitudinal heat flow. This method was implemented using a device for determining the thermal conductivity coefficient KIT-800 (Teplofon, Moscow, Russia). Thermal conductivity measurements were carried out according to the methodology for determining the change in the magnitude of the longitudinal heat flow passing through thin samples when they are heated, by measuring the temperature difference on thermocouples on both sides of the sample. At the same time, for the accuracy of measurements, all samples were measured before irradiation and numbered, so that in the future the contribution of accumulated radiation defects in the damaged layer to changes in the thermophysical parameters of the ceramics could be determined.

Testing of ceramic samples exposed to irradiation for thermal stability and retention of strength properties was carried out as follows. Ceramic samples were subjected to thermal heating to a temperature of 1000 °C, followed by exposure for 1 h and rapid cooling by removing the samples from the furnace chamber. These procedures make it possible to simulate the effects of thermal shock on samples that may occur during their operation. Similar heating and rapid cooling procedures were repeated for a total of 10 consecutive cycles, with hardness and crack resistance measurements conducted after each cycle. Ana-

lyzing the evolving trends in strength characteristics over the course of these thermal cycles enables us to ascertain the kinetics of resistance to high-temperature degradation.

3. Results and Discussion

When analyzing the resistance to gas swelling and the accumulation of implanted helium in the near-surface layer, the most effective approach involves evaluating alterations in structural parameters, notably crystal lattice parameters and volume. Assessing these parameter changes enables the determination of key kinetics of radiation damage accumulation within ceramics. It also helps identify the type of deformation resulting from radiation-induced crystal lattice distortions. The variation in structural parameters with irradiation fluence sheds light on ceramics' resistance to external factors and enables the estimation of degradation rates.

Table 1 presents the results of assessing changes in the structural parameters of the ceramics under study depending on the irradiation fluence, which were obtained by analyzing the X-ray diffraction patterns of the ceramic samples under study. It is important to highlight that the analysis of the studied samples with respect to irradiation fluence, utilizing the X-ray phase analysis method, revealed no signs of characteristic diffraction reflections associated with impurity inclusions. Determination of the crystal lattice parameters was carried out by a full-profile analysis of the position of the main diffraction maxima and their changes relative to the standard values (for Li_2TiO_3—PDF-00-033-0831, for Li_4SiO_4—PDF-01-070-2340, for Li_2ZrO_3—PDF-00-033-0843) chosen as references. The parameters were refined using the Diffrac EVA v.4.0 software code. This observation suggests the absence of phase or polymorphic transformation processes within the ceramics stemming from the accumulation of deformation distortions. Furthermore, this examination highlighted the resilience of the chosen ceramics to external factors linked to high-temperature irradiation. The main alterations are characteristic of deformation distortions of the crystal structure, which manifest themselves to varying degrees for different samples.

Table 1. Data on the crystal lattice parameters of the ceramics under study depending on the irradiation fluence.

Fluence, ion/cm^2	Li_4SiO_4	Li_2TiO_3	Li_2ZrO_3
	Lattice Parameter, Å		
Pristine	a = 11.54015 ± 0.00042; b = 6.07448 ± 0.00053; c = 16.60257 ± 0.00024; β = 99.285°; V = 1147.60 Å^3	a = 5.05409 ± 0.00018; b = 8.76622 ± 0.00014; c = 9.73412 ± 0.00032; β = 100.141°; V = 424.54 Å^3	a = 5.39574 ± 0.00017; b = 8.98502 ± 0.00018; c = 5.38123 ± 0.00031; β = 113.132°; V = 239.91 Å^3
1×10^{16} ion/cm^2	a = 11.53937 ± 0.00027; b = 6.08174 ± 0.00042; c = 16.62249 ± 0.00035; β = 99.405°; V = 1150.88 Å^3	a = 5.05813 ± 0.00036; b = 8.78022 ± 0.00034; c = 9.74968 ± 0.00035; β = 100.301°; V = 426.02 Å^3	a = 5.40219 ± 0.00025; b = 9.00656 ± 0.00028; c = 5.39198 ± 0.00021; β = 113.268°; V = 242.01 Å^3
5×10^{16} ion/cm^2	a = 11.54859 ± 0.00025; b = 6.09146 ± 0.00036; c = 16.64241 ± 0.00025; β = 99.485°; V = 1154.75 Å^3	a = 5.07102 ± 0.00024; b = 8.79571 ± 0.00036; c = 9.76689 ± 0.00031; β = 100.462°; V = 428.30 Å^3	a = 5.40867 ± 0.00027; b = 9.02816 ± 0.00028; c = 5.41133 ± 0.00021; β = 113.449°; V = 242.41 Å^3
1×10^{17} ion/cm^2	a = 11.55320 ± 0.00025; b = 6.09875 ± 0.00023; c = 16.68899 ± 0.00022; β = 99.603°; V = 1159.43 Å^3	a = 5.07910 ± 0.00024; b = 8.81677 ± 0.00024; c = 9.79419 ± 0.00016; β = 100.582°; V = 431.14 Å^3	a = 5.41947 ± 0.00024; b = 9.06787 ± 0.00028; c = 5.43509 ± 0.00032; β = 113.813°; V = 244.33 Å^3

Table 1. *Cont.*

Fluence, ion/cm^2	Li$_4$SiO$_4$	Li$_2$TiO$_3$	Li$_2$ZrO$_3$
	Lattice Parameter, Å		
3×10^{17} ion/cm^2	a = 11.56706 ± 0.00027; b = 6.11090 ± 0.00023; c = 16.73568 ± 0.00022; β = 99.683°; V = 1166.11 Å^3	a = 5.08722 ± 0.00022; b = 8.84493 ± 0.00027; c = 9.85443 ± 0.00025; β = 100.824°; V = 435.52 Å^3	a = 5.43243 ± 0.00026; b = 9.10407 ± 0.00023; c = 5.46113 ± 0.00024; β = 114.085°; V = 246.58 Å^3
5×10^{17} ion/cm^2	a = 11.58554 ± 0.00035; b = 6.12554 ± 0.00033; c = 16.61596 ± 0.00026; β = 99.844°; V = 1175.82 Å^3	a = 5.10143 ± 0.00026; b = 8.85192 ± 0.00024; c = 9.92141 ± 0.00018; β = 101.066°; V = 441.63 Å^3	a = 5.45196 ± 0.00026; b = 9.13319 ± 0.00023; c = 5.52893 ± 0.00025; β = 114.450°; V = 250.62 Å^3

The main changes in the structural parameters of the ceramics under study depending on the irradiation fluence indicate the occurrence of residual stresses in the damaged layer, which are not of a relaxation nature (data on structural changes were obtained immediately after irradiation and rechecked 3 months after irradiation). At the same time, the nature of changes in parameters and increase in volume with variations in irradiation fluence indicates deformation distortions of the stretching type (i.e., parameters increase), the accumulation of which is clearly visible with rising fluence, and the nature of accumulation itself is non-linear (i.e., when the fluence rises above 10^{17} ion/cm^2, the deformation distortion of the structure grows sharply). It is important to emphasize that this pattern is consistent across all three ceramic types, with the difference only in the magnitude of structural changes, reflecting deformation distortion and swelling of the crystal structure.

Using the information regarding alterations in the crystal lattice volume compared to the initial measurements of non-irradiated samples, the values of volumetric swelling (ΔV) were computed. The variation in ΔV, contingent on the irradiation fluence, is displayed in Figure 4. The overall trend depicted in this dependence highlights a tensile-type deformation distortion of the crystal lattice, stemming from the accumulation of structural changes linked to the modification of lattice parameters. It is evident that Li$_4$SiO$_4$ ceramics exhibit the highest resistance to swelling, with a maximum ΔV change of no more than 2.5% at an irradiation fluence of 5×10^{17} ion/cm^2, in contrast to the much greater ΔV change observed at this fluence. It is important to highlight that at lower irradiation fluences (10^{16}–10^{17} ion/cm^2), the variation in ΔV is less than 1%, which indicates a fairly high resistance to radiation damage linked to deformation distortions. The rise in ΔV at fluences exceeding 10^{17} ion/cm^2 can be attributed to the cumulative impact of ion concentration and potential agglomeration into gas-filled bubbles. Nevertheless, when compared to the findings in [26–28], irradiation at 1000 K results in more pronounced ceramics degradation, likely due to the heightened mobility and accelerated agglomeration of implanted helium at higher irradiation fluences [29,30]. The explanation for the change in the swelling value, which has a clearly non-linear character at high irradiation fluences, can be explained as follows. At low irradiation fluences, the accumulation of structural distortions associated with the interaction of incident ions with the crystal structure occurs quite slowly, since some of the resulting defects can be isolated from each other due to the small size of the damaged areas that arise along the trajectory of ion movement in the ceramic. Moreover, in the case of high irradiation temperatures (1000 K), due to changes in the amplitude of thermal vibrations of atoms, some of the resulting defects can be partially annihilated. As a result, structural changes associated with swelling of the crystal lattice are small and have an almost linear dependence on the irradiation fluence. At fluences above 10^{17} ion/cm^2, which are characterized by fairly large values of dpa (more than 3–8 dpa), structural distortions of the crystal lattice associated with the accumulation of damage, as well as atomic displace-

ments, become more pronounced, which leads to swelling of the crystal structure and a sharp increase in the value of ΔV. Also, an important role in these changes is played by the accumulation of implanted He^{2+} ions, which by their nature, have a fairly high mobility and the ability to agglomerate in voids, the formation of which is directly related to the deformation processes of distortion of the crystal lattice, as well as atomic displacements. The presence of pores in ceramics also contributes to the agglomeration of helium in them, which at high concentrations of helium (about 1–2 at. %) can lead to the effect of merging of small bubbles into larger agglomerates. This has a mechanical deformation effect on the crystal structure, which leads to its destruction. Moreover, according to the literature data [28–30], critical doses of irradiation with low-energy He^{2+} ions, which lead to the formation of gas-filled bubbles and, as a consequence, swelling of the crystal structure, are doses above 10^{17} ion/cm^2, which are characterized by the formation of blisters and partial degradation of the damaged layer. In turn, as shown in [26–28], the effects of swelling are also influenced by irradiation conditions (in particular, irradiation temperature). In this case, an increase in the irradiation temperature to 1000 K when irradiating samples leads to a more pronounced degradation of the crystal structure associated with its swelling. This effect can be explained by the increased mobility of implanted He^{2+} ions associated with high temperature, which leads to the faster agglomeration of small gas bubbles into larger ones, which is well known from the results of post-irradiation annealing of irradiated samples of steels and alloys irradiated with He^{2+} ions [31,32].
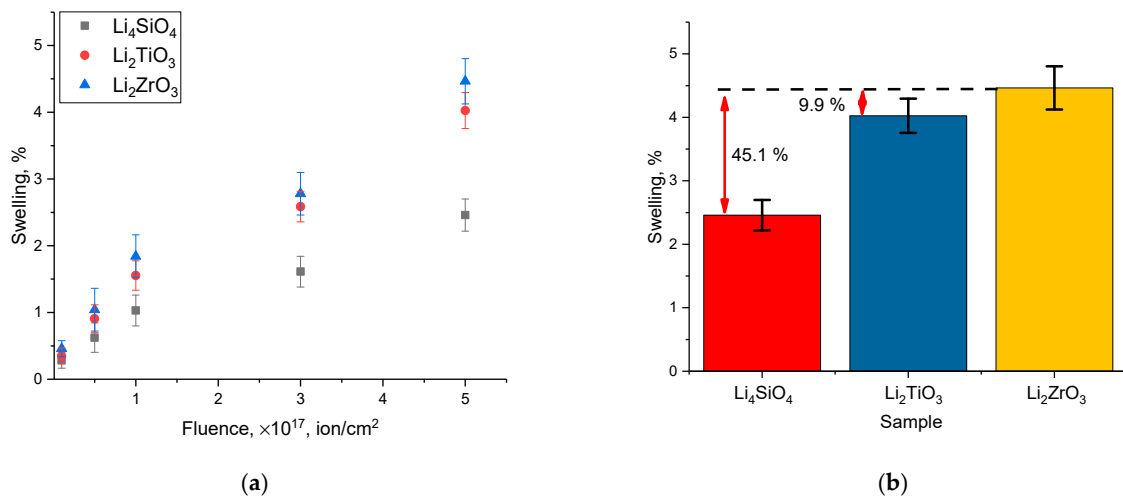
Figure 4. (**a**) The assessment results of the crystal lattice swelling value as a function of the irradiation fluence of lithium-containing ceramics; (**b**) the results of a comparative analysis of the maximum swelling value of ceramics at an irradiation fluence of 5×10^{17} ions/cm^2 (arrows indicate the difference in swelling of Li$_4$SiO$_4$ and Li$_2$TiO$_3$ ceramics in comparison with Li$_2$ZrO$_3$ ceramics).

Hence, when assessing the operational capabilities of lithium ceramics, it is essential to consider not only the accumulation of radiation damage, but also the temperature factor associated with the operating conditions.

The comparative analysis of crystal lattice swelling changes at the highest irradiation fluence (5×10^{17} ion/cm^2) reveals that Li$_4$SiO$_4$ ceramics exhibit the highest resistance to structural damage, with a swelling value not exceeding 2.5%. This represents a reduction of over 40% compared to Li$_2$TiO$_3$ and Li$_2$ZrO$_3$. Simultaneously, the disparity in swelling between Li$_2$TiO$_3$ and Li$_2$ZrO$_3$ does not exceed 10%, signifying limited resistance to swelling during helium accumulation. In this scenario, the substantial degradation of Li$_2$ZrO$_3$ can be attributed to the characteristics of anisotropic broadening of the crystal lattice under elevated temperature conditions. This, combined with irradiation effects and the heightened mobility of implanted helium, accelerate the degradation of ceramics [33,34].

The results of changes in hardness and resistance to a single compression depending on the irradiation fluence are presented in Figure 5. Based on the obtained data on alterations in hardness, the softening factor and crack resistance were assessed, the value of which determines the decrease in strength characteristics, alongside the degradation rate with the radiation damage accumulation. The data from the calculations performed are demonstrated in Figure 5c,d. Analysis of these alterations in hardness parameters revealed that Li_2TiO_3 and Li_2ZrO_3 have higher values in the initial state. This characterizes them as high-strength ceramics compared to Li_4SiO_4, for which the strength characteristics in the initial state are almost 10% lower than those of Li_2TiO_3 and Li_2ZrO_3 ceramics.
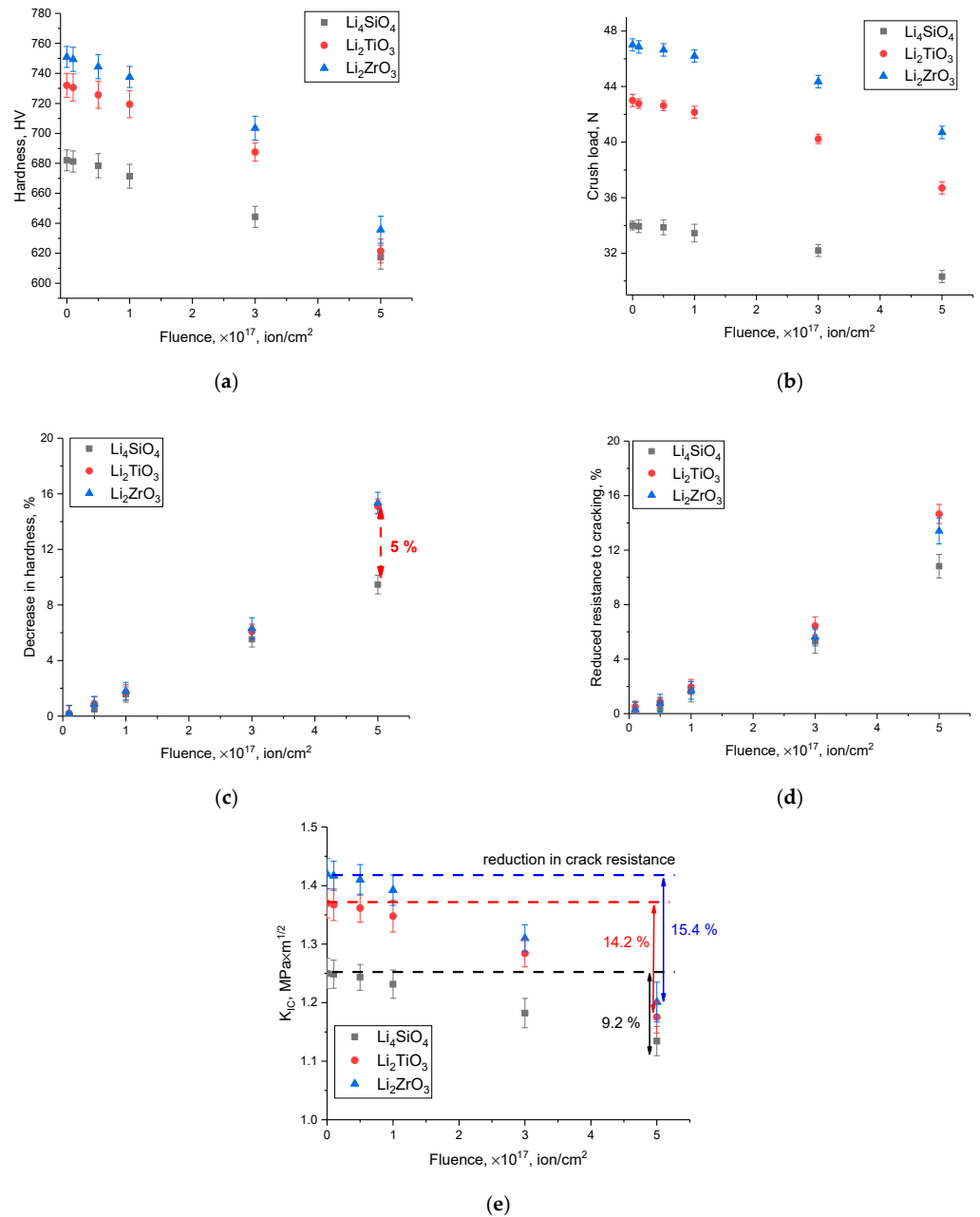
Figure 5. The results of alterations in strength characteristics: (**a**) variation in the hardness of ceramics; (**b**) the results of changes in the maximum pressure that ceramics can withstand during a single compression; (**c**) change in resistance to softening and decrease in hardness as a result of cracking of the surface layer; (**d**) results of changes in crack resistance and resistance to fracture under single compression; (**e**) assessment results of changes in the value of fracture toughness (crack resistance) depending on the value of irradiation fluence.

An overall assessment of the observed alterations in the strength properties of the examined ceramics can be categorized into two stages, each marked by distinct rates of strength degradation. At fluences ranging from 10^{16} to 10^{17} ion/cm^2, the shift in strength properties remained within the range from 1% to 2%. Remarkably, irrespective of the ceramic type, the character and extent of changes in hardness and single compression resistance fell within the same range of values during this stage. Elevated irradiation fluences exceeding 10^{17} ion/cm^2 result in a more pronounced softening of the ceramics, and as fluence increases, discernible differences in the patterns of strength parameter changes become apparent. Beyond 10^{17} ion/cm^2, the decline in strength properties is less pronounced for Li_4SiO_4 ceramics compared to the other two types, Li_2TiO_3 and Li_2ZrO_3, where the maximum reduction in strength parameters exceeds 12–15%, while for Li_4SiO_4, these changes are 4–5% lower. This difference may be due to the higher resistance of Li_4SiO_4 ceramics to swelling and subsequent destruction under high-dose irradiation, which is more pronounced for Li_2TiO_3 and Li_2ZrO_3 (see data on changes in structural parameters and ΔV values). When the deterioration of strength parameters for Li_2TiO_3 and Li_2ZrO_3 can be caused not only by the effects of accumulation of structural distortions during high-dose irradiation, but also by anisotropic distortion of the crystal lattice, this manifests itself at high fluences (see data on changes in crystal lattice parameters in Table 1). Figure 5e shows the results of changes in the value of fracture toughness (crack resistance), which reflect the change in the resistance of ceramics to cracking during the accumulation of radiation defects in the damaged layer, and characterize the dynamics of deterioration in the strength properties of ceramics exposed to irradiation. According to the data obtained, the maximum reduction in crack resistance for the studied ceramics at an irradiation fluence of 5×10^{17} ion/cm^2 is about 9.2% for Li_4SiO_4 ceramics, and about 14–15% for Li_2TiO_3 and Li_2ZrO_3 ceramics, which has good agreement with changes in hardness and resistance to cracking. In this case, as in the case of changes in strength properties, Li_4SiO_4 ceramics have the maximum resistance to cracking, for which the value of resistance at maximum damage fluence is about one and a half times in comparison with alterations in the crack resistance of Li_2TiO_3 and Li_2ZrO_3 ceramics.

Figure 6 illustrates the alterations in thermophysical parameters, specifically the thermal conductivity coefficient and heat loss values, in the studied ceramics as a function of irradiation fluence with He^{2+} ions, the accumulation of which results in destructive modifications in structural and strength parameters. Based on the presented data regarding the thermal conductivity coefficients of the examined ceramics, Li_2TiO_3 ceramics exhibit the lowest value, approximately 1.71–1.72 W/m·K, whereas Li_4SiO_4 and Li_2ZrO_3 ceramics have values around 1.8–1.82 W/m·K. This variance in values can be attributed primarily to the ceramics' phase composition and their structural characteristics inherent in dielectric ceramics.

The results of alterations in thermophysical parameters presented in Figure 6 reflect the tendency for heat transfer to deteriorate at high irradiation fluences (above 10^{17} ions/cm^2), which are characterized by the accumulation of atomic displacements above 1 dpa. In this case, the critical point of irreversible deterioration of thermophysical parameters is a fluence of 3×10^{17} ions/cm^2, in which the degradation of thermophysical parameters is more than 10%. Moreover, in the case of fluences less than 3×10^{17} ions/cm^2, the change in thermophysical parameters is less than 1–2%, which signifies that the greatest contribution to the degradation of the thermal conductivity characteristics of ceramics is made by effects associated with a destructive change in the crystal lattice volume as a result of the accumulation of atomic displacements and agglomeration of implanted helium into the damaged layer. It is important to highlight that, in contrast to alterations in strength characteristics at high irradiation fluences (the difference in hardness degradation and resistance to single compression for different samples was more than 5%), the degradation of thermophysical parameters for all three types of ceramics at maximum irradiation fluence is in the same range of values (17–20%). Thus, we can conclude that variations in thermophysical parameters, in contrast to strength characteristics, are destructively

influenced by the magnitude of atomic displacements, i.e., the accumulation of structural distortions caused by disordering of the crystal structure due to helium implantation into the damaged layer.
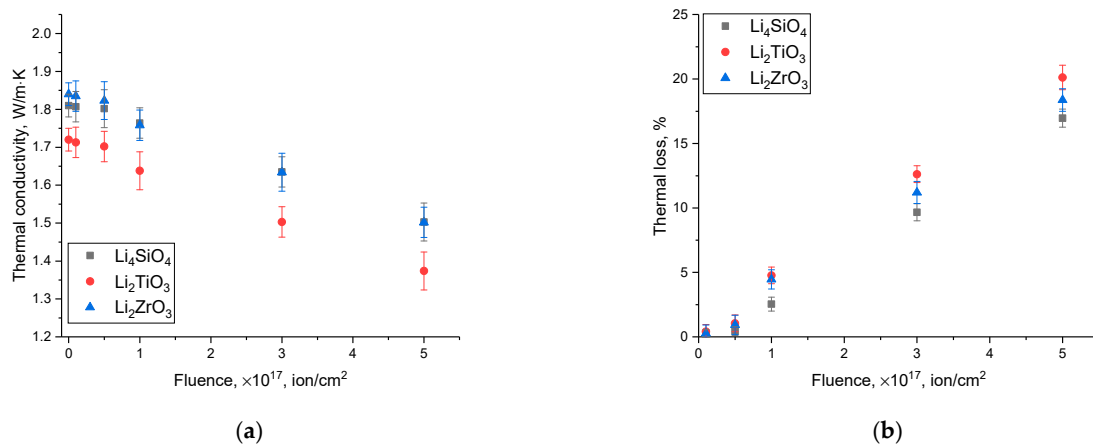
Figure 6. The results of changes in the thermophysical parameters of the ceramics under study as a function of the irradiation fluence: (**a**) change in the thermal conductivity coefficient of the ceramics; (**b**) change in heat losses (deterioration of thermal conductivity coefficient).

Figure 7 reveals the assessment results of the alteration in the strength characteristics of the three types of ceramics under study in the initial state and irradiated with maximum fluence (5×10^{17} ion/cm^2) during cyclic heat resistance tests (rapid heating to 1000 °C, exposure for 1 h, and removal to air). The depicted relationships reveal the ceramics' resistance to temperature fluctuations, which may, in turn, lead to degradation caused by oxidation and the emergence of additional distortions and residual mechanical stresses. Additionally, such assessments enable the identification of the materials most resistant to temperature variations and provide insights into how irradiation affects the preservation of strength property stability (degraded after irradiation).

A general analysis of the observed alterations in hardness values and the maximum pressure that ceramics can withstand to the stage of cracking during a single compression indicates that the most pronounced decrease in these values is observed after five cycles for irradiated samples (irradiation fluence was chosen 5×10^{17} ions/cm^2) and after seven to eight cycles in the case of the original ones (unirradiated samples). This difference in variations is primarily due to different rates of the high-temperature degradation of ceramics, which is linked to the mechanisms of oxygen penetration from the surface deep into the ceramics [35,36], thereby causing structural distortions and deformations leading to the initialization of the formation of microcracks in the structure. Secondly, the damaging deformation and distortion of the damaged ceramic layer, which take place during the implantation of helium, accelerate the degradation processes. It is crucial to note that helium, with its high mobility at elevated temperatures, can undergo rapid agglomeration, further intensifying the deformation distortions within the ceramic structure. This can be linked to the potential formation of gas-filled bubbles within the damaged layer [37,38]. The analogous occurrences of gas swelling due to thermal influence, linked to the accelerated agglomeration of helium and the formation of blisters, have been documented in several studies [39,40].

The results of a comparative analysis regarding the degradation of strength properties (hardness and crack resistance) are depicted in Figure 7c,d. These trends were derived from a comparative assessment of variations in strength characteristics both prior to testing and after 10 successive cycles, during which the most significant property deterioration was observed.

(**a**)

(**b**)

(**c**)

(**d**)
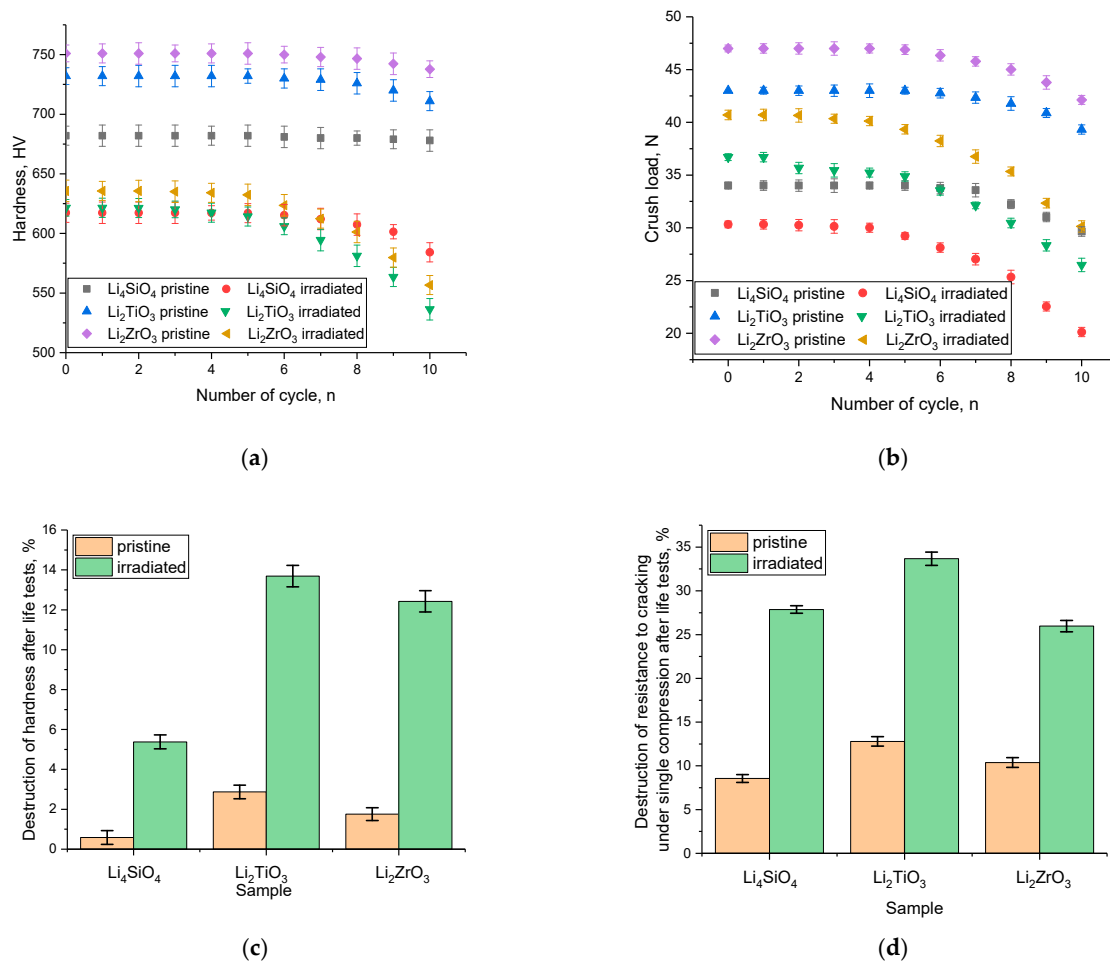
Figure 7. The assessment results of alterations in the strength properties of ceramics during cyclic tests for thermal resistance during high-temperature heating (data are given for samples in the initial state and irradiated with a maximum fluence of 5×10^{17} ion/cm^2): (**a**) the results of fluctuations in hardness; (**b**) the results of variation in the maximum pressure that ceramics can withstand during a single compression. The results of a comparative analysis of alterations in strength characteristics during heat resistance tests after 10 consecutive cycles, reflecting a destructive change in the properties of ceramics in the initial and irradiated states; (**c**) data on changes in hardness; (**d**) data on changes in crack resistance under a single compression.

As evident from the provided data concerning alterations in the strength properties of the examined ceramics following thermal resistance tests, the most resistant ceramics are the Li_4SiO_4 variety. In the absence of irradiation, these ceramics experienced a reduction in hardness of less than 1% compared to their initial values, and in irradiated samples, the decrease did not exceed 5% in comparison to the initial hardness. Conversely, for Li_2TiO_3 ceramics, the most significant changes in hardness values were observed, both in the case of the original (non-irradiated) samples and those subjected to irradiation. In the case of Li_2ZrO_3 ceramics, the decline in hardness is less significant when compared to Li_2TiO_3 ceramics, with a disparity in values of roughly 1–2%. This observation suggests a higher resistance to destructive high-temperature effects. However, for irradiated samples of Li_2TiO_3 and Li_2ZrO_3 ceramics, the alteration in hardness exceeds 10% following 10 successive cycles of heat resistance testing. Meanwhile, the pattern of variance in the reduction in hardness values between the untreated and irradiated samples persists across all three ceramic types. This suggests that the destruction processes triggered by temperature exposure share a similar character for all ceramic varieties.

Regarding crack resistance (resistance to fracture), the results obtained for both non-irradiated samples and those subjected to irradiation at the highest fluence (5×10^{17} ion/cm^2) and subsequent heat resistance tests indicate a more significant decline in resistance to damage for all examined specimens. This phenomenon could be attributed to the heating process to maximum temperature and rapid cooling, causing the migration of oxygen and helium ions. Consequently, this leads to their deeper penetration, thereby expanding the damaged layer and introducing additional structural distortions during their movement. Consequently, when subjected to external influence and increasing pressure, the processes of crack formation take place at significantly lower pressures. This is due to the higher concentration of deformation inclusions within the samples, which is considerably higher compared to samples that were solely irradiated. The accumulation of these deformation inclusions, in turn, initiates the formation of microcracks. When subjected to external pressure, these microcracks propagate rapidly within the samples, resulting in reduced resistance to destructive failure under load. This hypothesis, which highlights the alteration in the stability of irradiated samples following 10 consecutive cycles of heat resistance testing, is further substantiated by the findings regarding alterations in crack resistance observed in non-irradiated (initial) samples subjected to heat resistance testing. In the case of the initial samples, there is a general trend of crack resistance decreasing by approximately 8–12%, which is three to five times greater compared to the changes observed in hardness values. The noticeable discrepancy in the extent of alterations in strength characteristics following heat resistance tests signifies the accelerated degradation of ceramics under thermal stress conditions, such as rapid heating and cooling. This degradation is primarily attributed to a reduced crack resistance, resulting in the decrease in resistance to external mechanical loads. Furthermore, for irradiated samples in which structural distortions accumulate due to irradiation, exposure to heat amplifies the degradation process, causing a decline in crack resistance of over 25–30% when compared to irradiated samples not subjected to heat resistance tests.

4. Conclusions

The paper presents the assessment results of the resistance of lithium-containing ceramics to helium swelling and the subsequent destruction under high-temperature irradiation with He^{2+} ions and fluences of 10^{16}–5×10^{17} ion/cm^2, which makes it possible to simulate the structural damage accumulation of the order of 5–8 dpa. During the evaluation of structural and strength parameters, it became evident that the primary factor contributing to property degradation is the accumulation of helium and its subsequent accelerated swelling under high-dose irradiation. Notably, Li$_4$SiO$_4$ ceramics exhibited the highest resistance to structural disorder. An examination of alterations in the thermophysical characteristics of the studied ceramics revealed that a critical irradiation dose, marked by a significant decline in heat transfer efficiency, occurs at a fluence surpassing 3×10^{17} ion/cm^2. This threshold is characterized by the prevalence of atomic displacements and the effects associated with helium agglomeration in the damaged layer. Meanwhile, an alteration in the type of ceramics under maximum irradiation fluences does not result in substantial discrepancies in the resistance of thermophysical parameters to radiation disorder. Thermal resistance experiments indicated that the examined samples, when subjected to irradiation, can preserve the stability of their strength characteristics throughout three to five consecutive heating–cooling cycles. However, after the fifth cycle, a noticeable decline in strength parameters occurs, linked to the destabilization of the damaged layer and embrittlement (reduced crack resistance).

The obtained dependencies can be used in the future to develop operating modes for lithium-containing ceramics as blanket materials for tritium breeding.

Institutional Review Board Statement: Not applicable.

Informed Consent Statement: Not applicable.

Data Availability Statement: The data presented in this study are available in the article.

Conflicts of Interest: The authors declare no conflict of interest.

References

1. Duerrschnabel, M.; Gaisina, E.; Gaisin, R.; Walter, M.; Aktaa, J.; Rieth, M. Nanoscale insights into the corrosion of EUROFER by lithium ceramics. *Corros. Sci.* **2022**, *199*, 110190. [CrossRef]
2. Jiang, W.; Kovarik, L.; Wirth, M.G.; Zhu, Z.; Canfield, N.L.; Seymour, L.M.; Senor, D.J. Ion irradiation study of lithium silicates for fusion blanket applications. *J. Nucl. Mater.* **2023**, *576*, 154281. [CrossRef]
3. Zandi, N.; Sadeghi, H.; Habibi, M.; Jalali, I.; Zare, M. Blanket simulation and tritium breeding ratio calculation for ITER reactor. *J. Fusion Energy* **2015**, *34*, 1365–1368. [CrossRef]
4. Abou-Sena, A.; Ying, A.; Abdou, M. Effective thermal conductivity of lithium ceramic pebble beds for fusion blankets: A review. *Fusion Sci. Technol.* **2005**, *47*, 1094–1100. [CrossRef]
5. Ihli, T.; Basu, T.K.; Giancarli, L.M.; Konishi, S.; Malang, S.; Najmabadi, F.; Wu, Y. Review of blanket designs for advanced fusion reactors. *Fusion Eng. Des.* **2008**, *83*, 912–919. [CrossRef]
6. Leys, J.M.; Zarins, A.; Cipa, J.; Baumane, L.; Kizane, G.; Knitter, R. Radiation-induced effects in neutron-and electron-irradiated lithium silicate ceramic breeder pebbles. *J. Nucl. Mater.* **2020**, *540*, 152347. [CrossRef]
7. Cho, H.; Burgeson, I.E.; Adami, S.R.; Sinkov, S.I. Isotope-specific analysis of neutron-irradiated lithium aluminate ceramics by nuclear magnetic resonance spectroscopy. *J. Am. Ceram. Soc.* **2020**, *103*, 7291–7298. [CrossRef]
8. Chikhray, Y.; Shestakov, V.; Maksimkin, O.; Turubarova, L.; Osipov, I.; Kulsartov, T.; Tsuchiya, K. Study of Li_2TiO_3+ 5 mol% TiO_2 lithium ceramics after long-term neutron irradiation. *J. Nucl. Mater.* **2009**, *386*, 286–289. [CrossRef]
9. Ba, J.; Zeng, R.; Yan, X.; Li, R.; Wu, W.; Li, F.; Tang, T. Long-term helium bubble evolution in sequential He+ and H+ irradiated Li_4SiO_4. *Ceram. Int.* **2021**, *47*, 32310–32317. [CrossRef]
10. Szőcs, D.E.; Szilágyi, E.; Bogdán, C.; Kótai, E.; Horváth, Z.E. Lithium concentration dependence of implanted helium retention in lithium silicates. *Nucl. Instrum. Methods Phys. Res. Sect. B Beam Interact. Mater. At.* **2010**, *268*, 1857–1861. [CrossRef]
11. Sun, J.; You, Y.W.; Xu, Y.; Wu, X.; Li, B.S.; Liu, C.S. Interaction of irradiation-induced point defects with transmutants (H, He, Li, Be, B, Mg, Al and P) in 3C-SiC ceramics. *J. Eur. Ceram. Soc.* **2020**, *40*, 5196–5204. [CrossRef]
12. Avila, R.E.; Peña, L.A.; Jiménez, J.C. Surface desorption and bulk diffusion models of tritium release from Li_2TiO_3 and Li_2ZrO_3 pebbles. *J. Nucl. Mater.* **2010**, *405*, 244–251. [CrossRef]
13. Mukherjee, S.; Jamnapara, N.I. Materials research and development opportunities in fusion reactors. *Proc. Indian Natn. Sci. Acad.* **2015**, *81*, 827–839. [CrossRef]
14. Katsui, H.; Nagata, S.; Tsuchiya, B.; Shikama, T. Study on damage accumulation in $LiAlO_2$ single crystal irradiated with deuterium and helium ions by ion-channeling. *Nucl. Instrum. Methods Phys. Res. Sect. B Beam Interact. Mater. At.* **2010**, *268*, 2735–2739. [CrossRef]
15. Kenzhina, I.; Kulsartov, T.; Knitter, R.; Chikhray, Y.; Kenzhin, Y.; Zaurbekova, Z.; Nesterov, E. Analysis of the reactor experiments results on the study of gas evolution from two-phase Li_2TiO_3-Li_4SiO_4 lithium ceramics. *Nucl. Mater. Energy* **2022**, *30*, 101132. [CrossRef]
16. Kulsartov, T.; Zaurbekova, Z.; Knitter, R.; Shaimerdenov, A.; Chikhray, Y.; Askerbekov, S.; Ponkratov, Y. Studies of two-phase lithium ceramics Li_4SiO_4-Li_2TiO_3 under conditions of neutron irradiation. *Nucl. Mater. Energy* **2022**, *30*, 101129. [CrossRef]
17. Zinkle, S.J. Effect of H and He irradiation on cavity formation and blistering in ceramics. *Nucl. Instrum. Methods Phys. Res. Sect. B Beam Interact. Mater. At.* **2012**, *286*, 4–19. [CrossRef]
18. Fu, L.; Wang, B.; Zhu, Y.; Shen, T.; Deng, Y.; Xu, G.; Xia, W. Structural integrity and damage of glass-ceramics after He ion irradiation: Insights from ZrO_2-SiO_2 nanocrystalline glass-ceramics. *J. Eur. Ceram. Soc.* **2023**, *43*, 2624–2633. [CrossRef]
19. Zhang, H.; Su, R.; Shi, L.; O'Connor, D.J.; King, B.V.; Kisi, E.H. The damage evolution of He irradiation on Ti_3SiC_2 as a function of annealing temperature. *J. Eur. Ceram. Soc.* **2018**, *38*, 1253–1264. [CrossRef]
20. Huang, K.; Luo, L.M.; Zan, X.; Xu, Q.; Liu, D.G.; Zhu, X.Y.; Wu, Y.C. Microstructure and damage behavior of W–Cr alloy under He irradiation. *J. Nucl. Mater.* **2018**, *501*, 181–188. [CrossRef]
21. Sun, F.; Nakata, M.; Lee, S.E.; Zhao, M.; Wada, T.; Yamazaki, S.; Oya, Y. Synergistic effects of high energy helium irradiation and damage introduction at high temperature on hydrogen isotope retention in plasma facing materials. *J. Nucl. Mater.* **2020**, *533*, 152122. [CrossRef]
22. Li, B.; Liu, H.; Shen, T.; Xu, L.; Wang, J.; Zhao, F.; Xiong, A. Irradiation-induced microstructure damage in He-irradiated 3C-SiC at 1000 °C. *J. Eur. Ceram. Soc.* **2020**, *40*, 1014–1022. [CrossRef]
23. Su, R.; Zhang, H.; Shi, L.; Wen, H. Formation of nanostructures in Ti_2AlC induced by high-temperature helium irradiation. *J. Eur. Ceram. Soc.* **2019**, *39*, 1993–2002. [CrossRef]

24. Liu, C.; Shen, T.; Jin, P.; Wang, J.; Chang, H.; Zhu, Y.; Wang, Z. The role of He irradiation in the corrosion behaviour of T91 in high-temperature steam. *Corros. Sci.* **2021**, *189*, 109602. [CrossRef]

25. Tynyshbayeva, K.M.; Kozlovskiy, A.L.; Rakhimov, R.V.; Uglov, V.V.; Zdorovets, M.V. Study of The Gas-Swelling Mechanisms in Silicon Carbide Ceramics under High-Temperature Irradiation with Helium Ions. *Materials* **2023**, *16*, 5750. [CrossRef] [PubMed]

26. Zhou, Q.; Togari, A.; Nakata, M.; Zhao, M.; Sun, F.; Xu, Q.; Oya, Y. Release kinetics of tritium generation in neutron irradiated biphasic Li_2TiO_3–Li_4SiO_4 ceramic breeder. *J. Nucl. Mater.* **2019**, *522*, 286–293. [CrossRef]

27. Gu, S.; Ji, B.; Qi, Q.; Wang, J.; Zhou, H.S.; Zhang, Y.; Luo, G.N. Effects of He irradiation on the microstructure and mechanical performance of Li_2TiO_3. *Nucl. Fusion* **2021**, *61*, 106035. [CrossRef]

28. Abyshev, B.; Shlimas, D.I.; Zdorovets, M.V.; Arshamov, Y.K.; Kozlovskiy, A.L. Study of radiation resistance to helium swelling of Li_2ZrO_3/LiO and Li_2ZrO_3 ceramics. *Crystals* **2022**, *12*, 384. [CrossRef]

29. Huang, Z.; Zhou, M.; Cao, Z.; Tang, Z.; Zhang, Y.; Duan, J.; Wu, D. He irradiation-induced lattice distortion and surface blistering of $Gd_2Zr_2O_7$ defect-fluorite ceramics. *J. Am. Ceram. Soc.* **2020**, *103*, 3425–3435. [CrossRef]

30. Uglov, V.V.; Abadias, G.; Zlotski, S.V.; Saladukhin, I.A.; Cherenda, N.N. Surface blistering in ZrSiN nanocomposite films irradiated with He ions. *Surf. Coat. Technol.* **2020**, *394*, 125654. [CrossRef]

31. Li, Y.P.; Ran, G.; Liu, X.Y.; Qiu, X.; Han, Q.; Li, W.J.; Guo, Y.J. In-situ TEM observation of the evolution of helium bubbles in Mo during He+ irradiation and post-irradiation annealing. *Chin. Phys. B* **2021**, *30*, 086109. [CrossRef]

32. Levy, V.; Gilbon, D.; Rivera, C. *Influence of Helium on Swelling of Steels*; ASTM STP: Philadelphia, PA, USA, 1985; Volume 870, pp. 317–329.

33. Tokunaga, K.; Tamura, S.; Yoshida, N.; Ezato, K.; Taniguchi, M.; Sato, K.; Akiba, M. Synergistic effects of high heat loading and helium irradiation of tungsten. *J. Nucl. Mater.* **2004**, *329*, 757–760. [CrossRef]

34. Fan, C.; Pan, S.; Hu, X.; He, B.; Huang, M. Mechanisms of helium irradiation blistering and surface deformation in tungsten. *Acta Mater.* **2023**, *254*, 118993. [CrossRef]

35. Hoseini, A.; Malekian, A.; Bahrami, M. Deformation and thermal resistance study of aerogel blanket insulation material under uniaxial compression. *Energy Build.* **2016**, *130*, 228–237. [CrossRef]

36. Wilson, C.A.; Niven, B.E.; Laing, R.M. Estimating thermal resistance of the bedding assembly from thickness of materials. *Int. J. Cloth. Sci. Technol.* **1999**, *11*, 262–276. [CrossRef]

37. Liu, X.; Wu, Y.; Li, Y.; Ding, Y.; Liu, X.; Huang, J.; Ran, G. In situ studies on the evolution of damage microstructures in tungsten under heavy ion irradiation and post annealing. *Prog. Nucl. Energy* **2023**, *160*, 104677. [CrossRef]

38. Beyerlein, I.J.; Caro, A.; Demkowicz, M.J.; Mara, N.A.; Misra, A.; Uberuaga, B.P. Radiation damage tolerant nanomaterials. *Mater. Today* **2013**, *16*, 443–449. [CrossRef]

39. Shuster, D.L.; Farley, K.A. The influence of artificial radiation damage and thermal annealing on helium diffusion kinetics in apatite. *Geochim. Cosmochim. Acta* **2009**, *73*, 183–196. [CrossRef]

40. Guenthner, W.R.; Reiners, P.W.; Ketcham, R.A.; Nasdala, L.; Giester, G. Helium diffusion in natural zircon: Radiation damage, anisotropy, and the interpretation of zircon (U-Th)/He thermochronology. *Am. J. Sci.* **2013**, *313*, 145–198. [CrossRef]